# Catalytic Chemical Vapor Deposition Synthesis of Double-Walled and Few-Walled Carbon Nanotubes by Using a $MoO_3$-Supported Conditioning Catalyst to Control the Formation of Iron Catalytic Particles within an $\alpha$-$Al_{1.8}Fe_{0.2}O_3$ Self-Supported Foam

**Anne Cordier,[†] Valdirene G. de Resende,[†,‡] Alicia Weibel,[†] Eddy De Grave,[‡] Alain Peigney,[†] and Christophe Laurent*[,†]**

*Université de Toulouse, UMR UPS-CNRS-INPT, Institut Carnot CIRIMAT, Université Paul-Sabatier, 118 route de Narbonne, 31062 Toulouse cedex 9, France, and Department of Physics and Astronomy, University of Ghent, Proeftuinstraat 86, B-9000 Gent, Belgium*

$\alpha$-$Al_{1.8}Fe_{0.2}O_3$ and $\alpha$-$Al_{1.8}Fe_{0.2}O_3$−$MoO_3$ self-supported foams are used as catalytic materials for the synthesis of carbon nanotubes by catalytic chemical vapor deposition. A $MoO_3$-supported conditioning catalyst placed upstream in the reactor is more efficient than $MoO_3$ present within the catalytic material in producing double-walled and few-walled carbon nanotubes with fewer defects. It is shown that the corresponding modifications of the gas atmosphere (presence of $H_2O$ formed by the $H_2$ reduction of $MoO_3$ and, therefore, lower $H_2$ and $CH_4$ concentrations) allow one to limit more efficiently the release of the Fe catalyst from the oxide solid-solution foam, which results in the formation of fewer Fe nanoparticles, which, therefore, are less prone to undesirable growth. Thus, a $MoO_3$-induced "solid-state" effect is demonstrated within the catalytic material without molybdenum species being themselves present within this material. This could lead to simplifications in the design of catalytic materials.

## 1. Introduction

The catalytic chemical vapor deposition method is a very efficient technique for the large-scale and low-cost synthesis of carbon nanotubes. It is based on the catalytic decomposition of carbonaceous gases (usually CO, $CH_4$, $C_2H_4$, or $C_2H_2$) on a catalytic material that contains transition-metal (usually Fe or Co) nanoparticles. The addition of molybdenum species to the catalytic material allows greatly increasing the quantity of carbon nanotubes produced by this method. Several explanations have been proposed, implying a role of molybdenum species either in the solid phase or in the gas phase. First, several authors[1−4] have proposed that species, such as $Mo_2C$ or $MoO_3$ particles, are located around metal (Fe or Co) nanoparticles, therefore, isolating them from each other and limiting their coalescence. Thus, the addition of an adequate quantity of molybdenum should increase the number of metal nanoparticles active for carbon nanotube formation. It was also proposed[5] that the presence of molybdenum species makes it possible to decrease the synthesis temperature of single-walled nanotubes and, therefore, to limit the growth of metal nanoparticles and thus to decrease the single-walled nanotubes' diameters. However, the nature and location of the molybdenum species are not indicated. Second, it was shown[6−9] that the formation of mixed-phases, such as $CoMoO_4$, makes it possible to delay the reduction of the cobalt oxide, therefore, producing smaller and thus more active Co nanoparticles at the temperature of the carbon nanotube synthesis. It is important to note that, for all these explanations, it is stressed that the pure metal (Fe or Co) is the active species and that the in situ formed molybdenum carbide (mostly $Mo_2C$) is inactive. By contrast, some authors claimed that the active species are Fe−Mo alloys[10] or nonmagnetic alloys, such as $Fe_2Mo$ and Fe−Mo−C.[11,12] Other studies[13−16] simply mention Fe/Mo particles or "bimetallic" catalysts. As mentioned above, another explanation is that molybdenum species play no role in the solid phase but only favor some phenomena happening in the gas phase. Cassell et al.[17] have proposed that adding molybdenum species to Fe−$Al_2O_3$ catalysts favors the aromatization of $CH_4$ at high temperature and that, owing to the close proximity between molybdenum and iron catalytic sites where the growth of single-walled nanotubes takes place, the intermediate aromatic species can feed into the growth sites with high efficiency, without being limited by diffusion. In previous studies using the catalytic chemical vapor deposition method where the metal nanoparticles are formed in situ within the catalytic material, by selective reduction of an oxide solid solution,[18] we investigated the addition of molybdenum species to CoO−MgO[19−21] and $CoAl_2O_4$−$MgAl_2O_4$[22] solid solutions. It was found that it indeed increased the quantity of carbon nanotubes, but it was not possible to evidence any solid-state interaction between cobalt and molybdenum species. A further study showed that the addition of molybdenum species to an $\alpha$-$Al_{1.8}Fe_{0.2}O_3$ solid solution[23] favors the formation of double-walled nanotubes over that of single-walled nanotubes and activates smaller nanoparticles, thus producing smaller-diameter nanotubes. Moreover, a Mössbauer spectroscopy study evidenced that there are no interaction between iron and molybdenum species, pointing to a role of molybdenum favoring some phenomena happening in the gas phase, as opposed to any alloying effect. However, it was not possible to determine if the proximity between molybdenum and iron catalytic sites, as proposed by Cassell et al.,[17] is of key importance or not.

* To whom correspondence should be addressed. Tel: +33 (0)5 61 55 61 22. Fax: +33 (0)5 61 55 61 63. E-mail: laurent@chimie.ups-tlse.fr.

[†] Université de Toulouse, UMR UPS-CNRS-INPT, Institut Carnot CIRIMAT, Université Paul-Sabatier.

[‡] University of Ghent.

The use of a conditioning catalyst (also termed precatalyst) containing molybdenum species, such as $MoO_3$, was reported to increase the yield of single-walled nanotubes[24] or to favor the formation of high-quality double-walled nanotubes[25,26] and few-walled CNTs with 2−9 walls.[27,28] The conditioning catalyst would facilitate the transformation of $CH_4$ into more active species, promoting the formation of nanotubes on the downstream main catalytic material, that itself contained $MoO_3$ in addition to the usual catalysts (Fe or Co).[24−28] It is speculated[28] that the high selectivity for the formation of single-walled nanotubes originates from the near distance of the molybdenum and iron species, following Cassell et al.[17] Thus, the aim of this work is to compare the influence of molybdenum species present either within the catalytic material, as in all previous studies, or within a conditioning catalyst placed upstream during the catalytic chemical vapor deposition treatment. The catalytic materials are in the form of self-supported foams,[23,29−32] as opposed to powders, which is a promising way to ensure a good dispersion of the carbon nanotubes into ceramic foams that may have interesting characteristics that could be used for membrane applications.

## 2. Experimental Section

**2.1. Preparation of Powders and Self-Supported Foams.** A powder of $\alpha$-$Al_{1.8}Fe_{0.2}O_3$ solid solution was prepared by combustion and calcination in air at 1100 °C as detailed elsewhere.[30] This powder was divided into two batches, which were shaped into self-supported foams as described earlier.[23,32] The first batch was attrition-milled (2000 rpm, 3 h, alumina balls 200−300 $\mu$m in diameter) in ethanol with the addition of 1 mg of dispersant (Beycostat C213, CECA, France)/$m^2$ of powder. After rinsing in ethanol and filtering, the powder was dried in air and ground manually. A slurry composed of 35 wt % of the so-obtained powder and 65 wt % of (ethanol + dispersant) was homogenized by ultrasonic agitation (10 min). A polyurethane foam, 80 pores per inch (ppi), was impregnated by this slurry. The impregnated foam was mechanically pressed several times in order to eliminate the excess slurry. It was then dried overnight at room temperature and calcined in air (600 °C, 150 °C·$h^{-1}$, 60 min) in order to burn all organics, producing the $\alpha$-$Al_{1.8}Fe_{0.2}O_3$ self-supported foam. Two such foams were prepared. The second powder batch was used to prepare two more self-supported foams by the same route, except that an appropriate amount of ammonium heptamolybdate was dissolved into the slurry before impregnation of the polyurethane foam. The proportion of the element molybdenum compared to the total (iron + molybdenum) is equal to 5 mol %. In agreement with earlier results,[23,32] features corresponding solely to $\alpha$-$Al_{1.8}Fe_{0.2}O_3$ were detected for both self-supported foams by X-ray diffraction (Bruker D4 Endeavor, Cu K$\alpha$ radiation) and Mössbauer spectroscopy, confirming that there is no interaction between the molybdenum species ($MoO_3$) and the iron species ($\alpha$-$Al_{1.8}Fe_{0.2}O_3$). The BET specific surface area of all four foams is ca. 20 $m^2 \cdot g^{-1}$.

**2.2. Preparation of the Conditioning Catalyst.** The conditioning catalyst was prepared by soaking a commercial ceramic foam (Aluminum Martigny, France, 50 ppi, specific surface area lower than 1 $m^2 \cdot g^{-1}$, diameter = 32 mm, height = 22 mm) into a supersaturated aqueous solution (50 $g \cdot cm^{-3}$) of ammonium heptamolybdate. After draining, drying, and performing a calcination (500 °C, flowing air), a stable washcoat of $MoO_3$ was obtained on the walls of the ceramic foam.

**2.3. Synthesis of Carbon Nanotubes.** The four self-supported foams were transformed into carbon-nanotube-containing composite foams by a catalytic chemical vapor deposition treatment. It was performed in a silica reactor (inner diameter = 56 mm, length of the heating zone = 200 mm) using a $H_2-CH_4$ gas mixture (20 mol % $CH_4$), either without or with the presence of the upstream-positioned conditioning catalyst. The heating and the cooling rates to the desired temperature (1025 °C) and back to room temperature were 5 °C/min. No dwell time was applied at 1025 °C. The flowing gas was dried on $P_2O_5$, and its composition was regulated by mass-flow controllers. The nanotube-containing foam produced using the $\alpha$-$Al_{1.8}Fe_{0.2}O_3$ (i.e., molybdenum-free) foams will be denoted as F and M/F for catalytic chemical vapor deposition treatments without and with the upstream conditioning catalyst, respectively. Similarly, the specimens produced using the molybdenum-containing foams will be denoted as FM and M/FM.

**2.4. Characterization.** X-ray diffraction patterns were recorded in the range of 10−70° ($2\theta$) with a Bruker D4 Endeavor diffractrometer operating with Cu K$\alpha$ radiation. Counts were registered every 0.02° ($2\theta$). Mössbauer spectra were collected at 15 K using a spectrometer operating in constant acceleration mode with a triangular reference signal. A $^{57}$Co (Rh) source was used. Accumulation of data was made in 1024 channels. The spectra were computer analyzed in terms of model-independent distributions of hyperfine-parameter values, and numerical data quoted hereafter refer to maximum-probability values.[33] Isomer shifts are referenced with respect to $\alpha$-Fe at room temperature. The carbon content ($C_n$) in the composite foams was measured by the flash combustion method with an accuracy of ±2%. Raman spectra were recorded using a LabRAM 800 Jobin-Yvon spectrometer (632.82 nm) and were averaged on three spectra. The specimens were observed by field-emission-gun scanning electron microscopy (JEOL JSM 6700F). The observations were performed with a tension of 5 kV and a work distance between 4.0 and 6.2 mm, using the in-lens detector. High-resolution transmission electron microscopy was performed with a JEOL JEM 2100F microscope operated at 200 kV. The samples were slightly sonicated in ethanol, and a drop of the suspension was deposited onto a holey carbon grid.

## 3. Results and Discussion

The X-ray diffraction patterns (not shown) of all four composite foams show peaks corresponding to $\alpha$-$Al_2O_3$, $\alpha$-Fe, and $Fe_3C$, without any significant difference between the materials. $\gamma$-Fe or a $\gamma$-Fe−C alloy may be also present, but cannot be resolved on the patterns because the $\gamma$-Fe(111) diffraction peak ($d_{111}$ = 0.208 nm) is masked by the corundum (113) ($d_{113}$ = 0.209 nm) and the $Fe_3C$(121) ($d_{121}$ = 0.210 nm) peaks. Peaks of Fe−Mo carbides or Fe−Mo alloys were not detected. However, it is not possible to rule out their presence because the most intense diffraction peaks of these phases are close to those for $\alpha$-$Al_2O_3$ or $Fe_3C$. In addition, $\alpha$-$Mo_2C$ is detected for FM and M/FM. $MoO_3$ was not detected, suggesting that it was totally reduced during the catalytic chemical vapor deposition treatment.

Four components were required to obtain adequate fits of the Mössbauer spectra (Figure 1): (i) an $Fe^{3+}$ doublet representing the iron ions substituting for $Al^{3+}$ ions in the corundum lattice; (ii) an outer sextet with hyperfine parameters typical of the $\alpha$-Fe phase; (iii) an inner sextet that could be attributed to $Fe_3C$; and (iv) a central singlet due to a $\gamma$-Fe phase, possibly alloyed with carbon. The numerical results from the adjustments to the spectra are listed in Table 1. The effects upon the various hyperfine parameters when element molybdenum was added to the self-supported foam (specimens FM and M/FM) are minor and

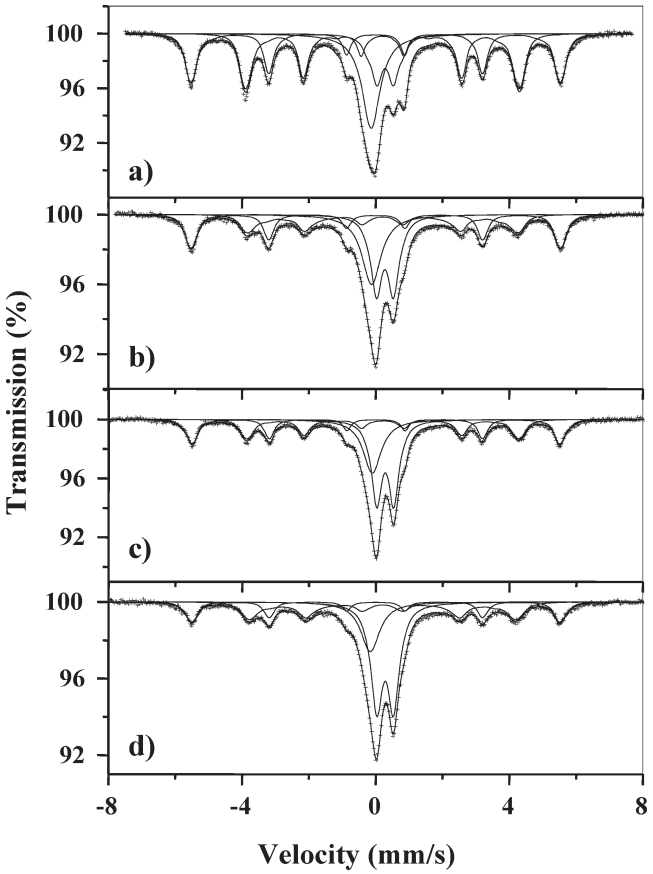


**Figure 1.** Mössbauer spectra (15 K) of the composite foams F (a), FM (b), M/F (c), and M/FM (d).

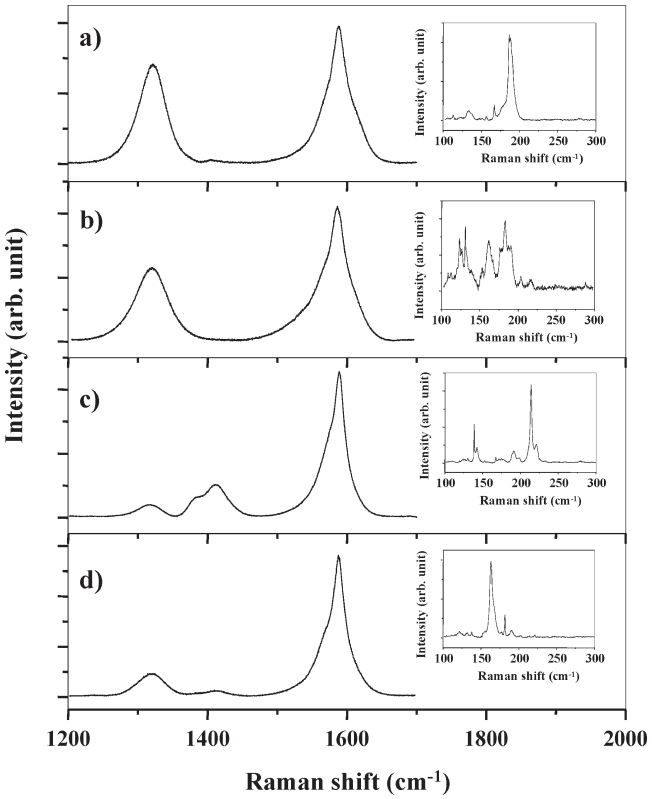


**Figure 2.** High-frequency range of the Raman spectra showing the D and G bands for composite foams F (a), FM (b), M/F (c), and M/FM (d) and (inset) the corresponding low-frequency range showing the radial-breathing-mode peaks.

mostly insignificant. This demonstrates that, after the catalytic chemical vapor deposition treatment, there is no solid−solid interaction between iron and molybdenum, and notably no alloying effect, in agreement with earlier findings.[23] In addition, the similarity between the four spectra makes it possible to directly compare the relative abundance (Table 1) of the various components. Interestingly, the relative abundance of the $Fe^{3+}$ doublet for F (15%) is lower than that for FM (28%) and is also lower for M/F (35%) than that for M/FM (42%), indicating that the selective reduction of the α-$Al_{1.8}Fe_{0.2}O_3$ solid solution is slightly inhibited when $MoO_3$ is present in the catalytic material (specimens FM and M/FM). Moreover, these values indicate that the selective reduction is very significantly inhibited when the conditioning catalyst is present (specimens M/F and M/FM).

The carbon content ($C_n$) in the foams is equal to 3.0 and 4.2 wt % for F and FM, respectively, and to 3.3 and 7.1 wt % for M/F and M/FM, respectively, showing that the presence of $MoO_3$ in the catalytic material markedly favors carbon deposition. The high-frequency range of the Raman spectra (Figure 2) shows the D band (ca. 1310 $cm^{-1}$) and the G band (ca. 1590 $cm^{-1}$). The ratio between their intensities, $I_{D/G}$, is high for F (72%), lower for FM (54%), and, interestingly, much lower for M/F (8%) and M/FM (16%), which is in qualitative agreement with the results reported by Liu et al.[28] A decreasing $I_{D/G}$ value corresponds to a lower proportion of $sp^3$-like carbon, which is generally attributed to the presence of fewer structural defects for the carbon nanotubes. Peaks at 1400 and 1420 $cm^{-1}$ were attributed to a photoluminescence effect of the $Fe^{3+}$ ions still present in the α-alumina lattice.[34] The presence of radial-breathing-mode peaks in the low-frequency range (100−300 $cm^{-1}$) of the Raman spectra (insets in Figure 2) is usually the sign of small-diameter nanotubes, such as single-walled and double-walled nanotubes. The peak frequencies are inversely proportional to the nanotubes' diameters. According to calculations, the detected diameters are in the range of 0.9−2.2 nm. Note, however, that the Raman process is influenced by optical

**TABLE 1: Mössbauer Parameters (15 K) for the Composite Foams[a]**

| | | | $Fe^{3+}$ | | | α-Fe | | | γ-Fe/C | | $Fe_3C$ | | |
|---|---|---|---|---|---|---|---|---|---|---|---|---|---|
| sample | catalytic material | conditioning catalyst | $\Delta E_{Q,m}$ | δ | RA | $B_{hf,m}$ | δ | RA | δ | RA | $B_{hf,m}$ | δ | RA |
| F | α | no | 0.50 | 0.40 | 15 | 34.3 | 0.12 | 29 | −0.03 | 23 | 25.5 | 0.32 | 33 |
| FM | α + $MoO_3$ | no | 0.51 | 0.40 | 28 | 34.3 | 0.12 | 25 | 0.00 | 23 | 25.1 | 0.32 | 24 |
| M/F | α | yes | 0.51 | 0.40 | 35 | 34.1 | 0.11 | 22 | 0.01 | 21 | 25.3 | 0.32 | 22 |
| M/FM | α + $MoO_3$ | yes | 0.50 | 0.40 | 42 | 34.1 | 0.12 | 16 | −0.04 | 17 | 24.8 | 0.32 | 25 |

[a] α = α-$Al_{1.8}Fe_{0.2}O_3$. The quadrupole splitting ($\Delta E_Q$) and isomer shifts (δ) are given in mm/s, the hyperfine fields ($B_{hf,m}$) are in T, and the relative spectral areas (RA) are in %. The quadrupole shifts for α-Fe and $Fe_3C$ and the quadrupole splitting for γ-Fe have been fixed at 0 mm/s. The hyperfine fields are for the maximum probability values ($B_{hf,m}$). Estimated errors in the quadrupole splittings and isomer shifts are 0.02 and 0.01 mm/s, respectively. For the relative spectral areas, the error is about 4% of the actual values, and for the hyperfine field, it is 0.2 T.

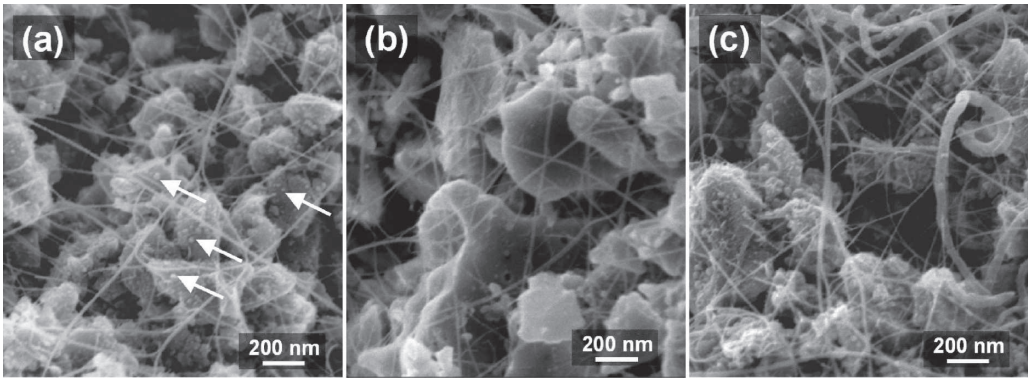


**Figure 3.** Field-emission-gun scanning electron microscopy images of the foams F (a), M/F (b), and M/FM (c).

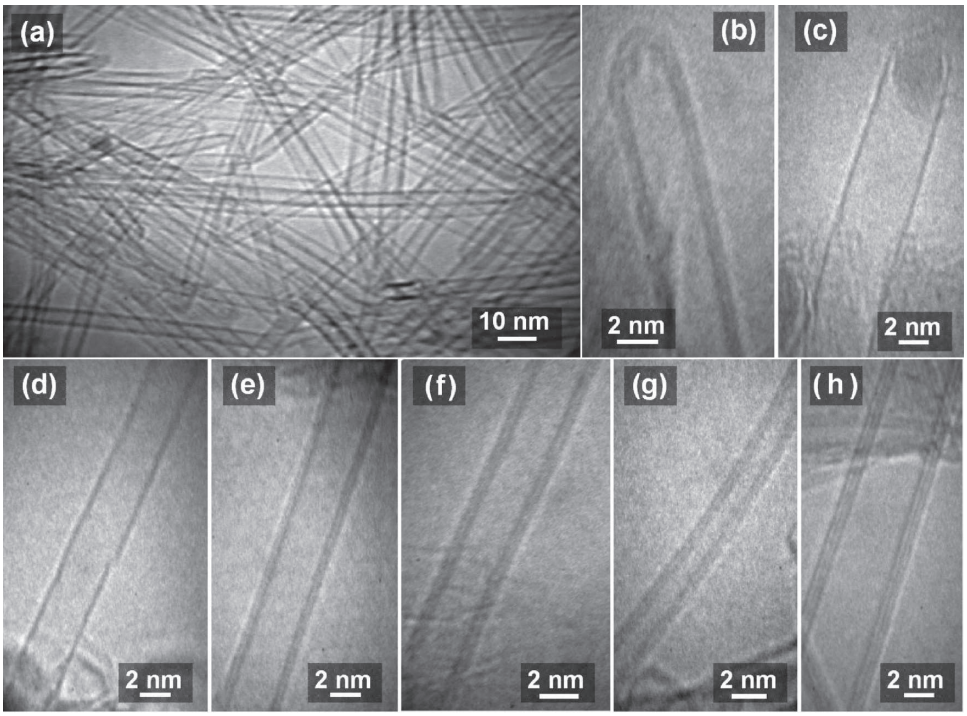


**Figure 4.** Typical transmission electron microscopy (a) and high-resolution transmission electron microscopy (b−h) images of carbon nanotubes in M/F.

resonance, and it is thus impossible to detect all existing carbon nanotubes using only one wavelength. Moreover, the peak intensities do not reflect the real amount of individual nanotubes because the resonance effect amplifies the Raman signals from certain nanotubes.

Field-emission-gun scanning electron microscopy images (Figure 3) reveal the presence of long, flexible filaments, with a smooth and regular surface, on the surface of the oxide grains and bridging several grains. All these filaments have a diameter smaller than 30 nm and a length of some tens of micrometers. From earlier results, it is known that such filaments are isolated nanotubes and/or nanotube bundles. The quantity of nanotubes is almost the same in samples F, M/F, and M/FM (Figure 3a−c) and FM (not shown). Spherical nanoparticles (arrowed in Figure 3a) that may be α-Fe, $\gamma$-Fe, and/or $Fe_3C$ are observed at the surface of the alumina grains, in a fairly large amount for F. Most of these particles, the diameter of which ranges between 5 and 20 nm, do not appear to be connected to a carbon nanotube, indicating that they have been inactive. Moreover, carbon nanofibers with a diameter in the range of 20−30 nm are observed for M/FM (Figure 3c), which is a indication that large metal particles have been activated and could, in part, reflect the higher carbon content for this material. All samples were studied by high-resolution transmission electron microscopy. Typical images for M/F reveal that the observed carbon nanotubes are clean (Figure 4a) with tips either empty (Figure 4b) or containing a catalytic particle (Figure 4c). The carbon nanotubes are mostly single-walled (Figure 4c,d) and double-walled (Figure 4b,e−g), and some have three walls (Figure 4h) or more (maximum of six walls). The distributions of the number of walls (Figure 5) were obtained from similar images. For F (Figure 5a), the proportion of single-walled carbon nanotubes is close to 70%, but for FM (Figure 5b), it is much lower (close to 50%), whereas the proportion of double-walled carbon nanotubes has increased to 40%, in agreement with earlier results.[23] This trend continues for M/F (Figure 5c) and M/FM (Figure 5d) and is accompanied by the steady increase of the proportion of triple-walled carbon nanotubes. This evolution, which is more progressive than the one reported by other authors,[27,28] is reflected by the average number of walls: 1.43, 1.68, 1.87, and 2.36 for F, FM, M/F, and M/FM, respectively. The diameter distributions for single-walled and double-walled carbon nanotubes (not shown) were plotted for each specimen. The average single-walled nanotube diameter is equal to 2.2

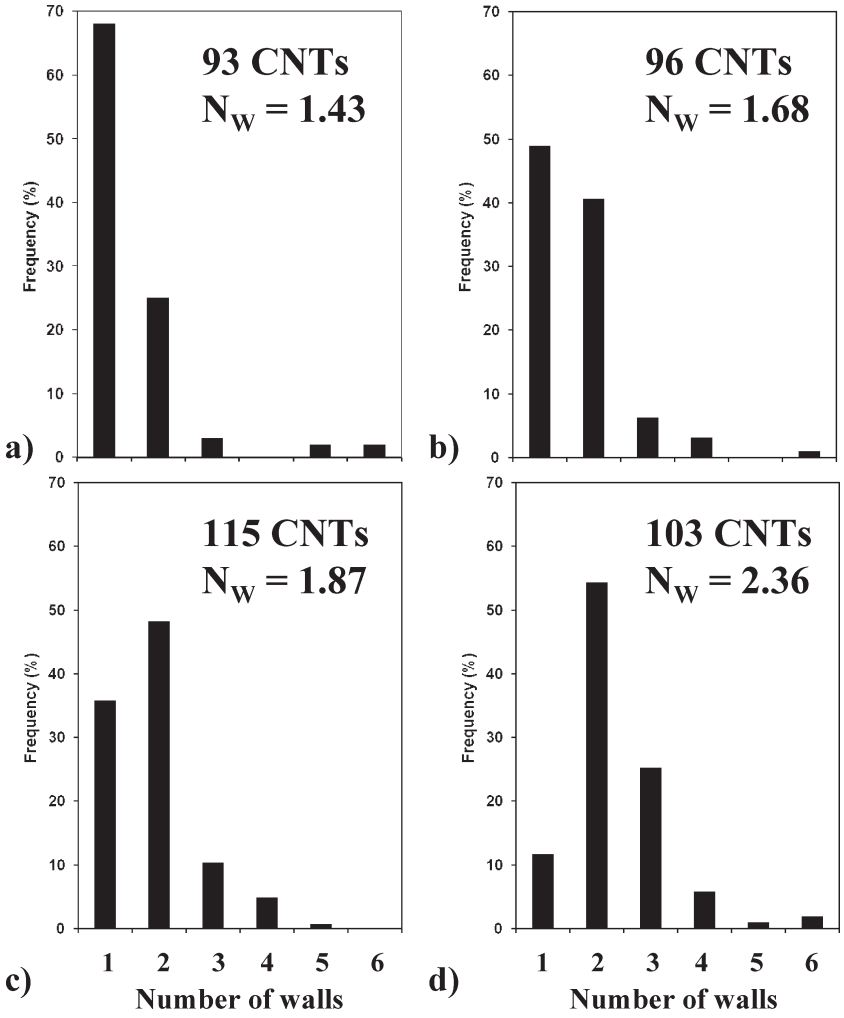


**Figure 5.** Distribution of the number of walls of carbon nanotubes in composite foams F (a), FM (b), M/F (c), and M/FM (d). $N_w$ is the average number of walls.

nm for F and M/F and 2.6 nm for FM and M/FM, showing no such an effect of the conditioning catalyst, whereas the $MoO_3$ present within the catalytic material tends to activate slightly larger Fe particles. The latter result could reflect the near distance of the molybdenum and iron species in the catalytic material, by contrast to other studies[17,28] where this proximity resulted in a higher selectivity toward single-walled carbon nanotubes. It is also noteworthy that, for a given sample, the average inner diameter of the double-walled carbon nanotubes is equal to or lower than the average diameter of the single-walled carbon nanotubes, supporting the yarmulke mechanism,[35,36] a base-growth mechanism according to which the second nanotubes' cap is formed underneath the first one during the nucleation stage that precedes the simultaneous growth of the two walls.

Clearly, all the results obtained for sample M/F support the previous findings[23] that interactions between iron and molybdenum species, such as alloying effects, are not mandatory to explain differences in nanotube selectivity or yield. As revealed by the Mössbauer spectroscopy results, the conditioning catalyst hampers the selective reduction of $\alpha$-$Al_{1.8}Fe_{0.2}O_3$, probably because the reduction−carburization of $MoO_3$ to $Mo_2C$ produces $H_2O$ and, therefore, decreases the concentrations of $H_2$ and $CH_4$ in the gas flow. Thus, the formation, by $H_2$ reduction of the $Fe^{3+}$ ions, of pristine Fe nanoparticles at the surface and in the open porosity of the alumina grains[37] is limited. Their undesirable growth will, therefore, be limited too, and they will stay at a size, below ca. 5 nm in diameter, appropriate for the formation of single-walled, double-walled, and few-walled carbon nanotubes via the yarmulke mechanism.[35,36] Moreover, the so-produced $H_2O$ could etch away carbon precipitates covering the Fe nanoparticles,[38,39] leading to cleaner and more active Fe nanoparticles and producing preferentially double-walled and few-walled carbon nanotubes with fewer defects, in agreement with the results obtained by high-resolution transmission electron microscopy and Raman spectroscopy. The conditioning catalyst also dissociates $CH_4$ to $C_1$ reactive species, such as $CH_3^+$ and $CH_2^{2+}$, which subsequently form reactive $C_2$ species that could be converted to some inactive aromatic or larger polycyclic aromatic hydrocarbon molecules.[28] For the specimen prepared using the conditioning catalyst but also containing $MoO_3$ within the catalytic material (M/FM), there might be some reactivation of these species.[40] The resulting excessive abundance of reactive carbon species would trigger the activation of much larger Fe particles, producing undesirable carbon nanofibers in addition to the carbon nanotubes, which could account for the higher carbon content in this specimen.

## 4. Conclusions

$\alpha$-$Al_{1.8}Fe_{0.2}O_3$ and $\alpha$-$Al_{1.8}Fe_{0.2}O_3$−$MoO_3$ self-supported foams were used as catalytic materials for the synthesis of carbon nanotubes by catalytic chemical vapor deposition. The influence of the presence of a $MoO_3$-supported conditioning catalyst placed upstream in the reactor was investigated. The condition-

ing catalyst is more efficient than $MoO_3$ present within the catalytic material in producing double-walled and few-walled carbon nanotubes, with fewer defects. Indeed, it allows one to control the carbon source, as was known previously, but in addition, it is shown that the corresponding modifications of the gas atmosphere (presence of $H_2O$ formed by the $H_2$ reduction of $MoO_3$ and, therefore, lower $H_2$ and $CH_4$ concentrations) make for a less reducing atmosphere, permitting limiting more efficiently the release of the Fe catalyst from the oxide solid-solution foam. The limited release will result in the formation of fewer Fe nanoparticles, which, therefore, are less prone to undesirable growth. To the best of our knowledge, this is the first time that such a molybdenum-induced "solid-state" effect within the catalytic material is demonstrated without molybdenum species being themselves present within this material. In addition, $H_2O$ produced from the decomposition of $MoO_3$ to $Mo_2C$ could etch away carbon precipitates covering the Fe nanoparticles, leading to more active nanoparticles. It is beneficial to use only the conditioning catalyst and a molybdenum-free catalytic material, in order to avoid an excessive abundance of reactive carbon species that would trigger the activation of larger Fe particles, producing undesirable carbon nanofibers in addition to the carbon nanotubes. These results could lead to important simplifications in the design of catalytic materials used in catalytic chemical vapor deposition routes.

**Acknowledgment.** This work was partially funded by the Fund for Scientific Research-Flanders and by the Special Research Fund (BOF, Bijzonder Onderzoeksfonds), UGent (B/06633), Belgium. The authors would like to thank Mr. L. Datas for assistance in high-resolution transmission electron microscopy observations. All electron microscopy observations were performed at TEMSCAN, the "Service Commun de Microscopie Electronique à Transmission", Université Paul Sabatier, Toulouse, France.

## References and Notes

(1) Tang, S.; Zhong, Z.; Xiong, Z.; Sun, L.; Liu, L.; Lin, J.; Shen, Z. X.; K.L., T. *Chem. Phys. Lett.* **2001**, *350*, 19–26.
(2) Li, Q.; Yan, H.; Cheng, Y.; Zhang, J.; Liu, Z. *J. Mater. Chem.* **2002**, *12*, 1179–1183.
(3) Mehn, D.; Fonseca, A.; Bister, G.; Nagy, J. B. *Chem. Phys. Lett.* **2004**, *393*, 378–384.
(4) Ago, H.; Uehara, N.; Yoshihara, N.; Tsuji, M.; Yumura, M.; Tomonaga, N.; Setoguchi, T. *Carbon* **2006**, *44*, 2912–2918.
(5) Harutyunyan, A. R.; Pradhan, B. K.; Kim, U. J.; Chen, G.; Eklund, P. C. *Nano Lett.* **2002**, *2*, 525–530.
(6) Kitiyanan, B.; Alvarez, W. E.; Harwell, J. H.; Resasco, D. E. *Chem. Phys. Lett.* **2000**, *317*, 497–503.
(7) Alvarez, W. E.; Kitiyanan, B.; Borgna, A.; Resasco, D. E. *Carbon* **2001**, *39*, 547–558.
(8) Zhou, L.-P.; Ohta, K.; Kuroda, K.; Lei, N.; Matsuishi, K.; Gao, L.; Matsumoto, T.; Nakamura, J. *J. Phys. Chem. B* **2005**, *109*, 4439–4447.
(9) Hart, A. J.; Slocum, A. H.; Royer, L. *Carbon* **2006**, *44*, 348–359.
(10) Li, Y.; Liu, J.; Wang, Y.; Wang, Z. L. *Chem. Mater.* **2001**, *13*, 1008–1014.
(11) Shah, N.; Pattanaik, S.; Huggins, F. E.; Panjala, D.; Huffman, G. P. *Fuel Process. Technol.* **2003**, *83*, 163–173.
(12) Punnoose, A.; Shah, N.; Huffman, G. P.; Seehra, M. S. *Fuel Process. Technol.* **2003**, *83*, 263–273.
(13) Hafner, J. H.; Bronikowski, M. J.; Azamian, B. R.; Nikolaev, P.; Rinzler, A. G.; Colbert, D. T.; Smith, K. A.; Smalley, R. E. *Chem. Phys. Lett.* **1998**, *296*, 195–202.
(14) Su, M.; Zheng, B.; Liu, J. *Chem. Phys. Lett.* **2000**, *322*, 321–326.
(15) Lyu, S. C.; Liu, B. C.; Lee, T. J.; Liu, Z. Y.; Yang, C. W.; Park, C. Y.; Lee, C. J. *Chem. Commun.* **2003**, 734–736.
(16) Seidel, R.; Duesberg, G. S.; Unger, E.; Graham, A. P.; Liebau, M.; Kreupl, F. *J. Phys. Chem. B* **2004**, *108*, 1888–1893.
(17) Cassell, A. M.; Raymakers, J. A.; Kong, J.; Dai, H. *J. Phys. Chem. B* **1999**, *103*, 6484–6492.
(18) Peigney, A.; Laurent, Ch.; Dobigeon, F.; Rousset, A. *J. Mater. Res.* **1997**, *12*, 613–615.
(19) Flahaut, E.; Bacsa, R.; Peigney, A.; Laurent, Ch. *Chem. Commun.* **2003**, 1442–1443.
(20) Flahaut, E.; Peigney, A.; Bacsa, W. S.; Bacsa, R. R.; Laurent, Ch. *J. Mater. Chem.* **2004**, *14*, 646–653.
(21) Flahaut, E.; Laurent, Ch.; Peigney, A. *Carbon* **2005**, *43*, 375–383.
(22) Rul, S.; Lefèvre-Schlick, F.; Capria, E.; Laurent, Ch.; Peigney, A. *Acta Mater.* **2004**, *52*, 1061–1067.
(23) Cordier, A.; de Resende, V. G.; De Grave, E.; Peigney, A.; Laurent, Ch. *J. Phys. Chem. C* **2008**, *112*, 18825–18831.
(24) Franklin, N. R.; Dai, H. J. *Adv. Mater.* **2000**, *12*, 890–894.
(25) Endo, M.; Muramatsu, H.; Hayashi, T.; Kim, Y. A.; Terrones, M.; Dresselhaus, M. S. *Nature* **2005**, *433*, 476.
(26) Kim, Y. A.; Muramatsu, H.; Hayashi, T.; Endo, M.; Terrones, M.; Dresselhaus, M. S. *Chem. Vap. Deposition* **2006**, *12*, 327–330.
(27) Liu, Y. F.; Takeuchi, K.; Park, K. C.; Muramatsu, H.; Fukuyo, T.; Endo, M. *J. Mater. Res.* **2009**, *24*, 1307–1310.
(28) Liu, Y. F.; Wongwiriyapan, W.; Park, K. C.; Muramatsu, H.; Takeuchi, K.; Kim, Y. A.; Endo, M. *Carbon* **2009**, *47*, 2543–2546.
(29) Rul, S.; Laurent, Ch.; Peigney, A.; Rousset, A. *J. Eur. Ceram. Soc.* **2003**, *23*, 1233–1241.
(30) Cordier, A.; Flahaut, E.; Viazzi, C.; Laurent, Ch.; Peigney, A. *J. Mater. Chem.* **2005**, *15*, 4041–4050.
(31) Cordier, A.; Rossignol, F.; Laurent, Ch.; Chartier, T.; Peigney, A. *Appl. Catal., A* **2007**, *319*, 7–13.
(32) de Resende, V. G.; De Grave, E.; Cordier, A.; Weibel, A.; Peigney, A.; Laurent, Ch. *Carbon* **2009**, *47*, 482–492.
(33) Vandenberghe, R. E.; De Grave, E.; de Bakker, P. M. A. *Hyperfine Interact.* **1994**, *83*, 29–49.
(34) Lemoine, P.; Quinn, J. P.; Maguire, P.; McLaughlin, J. A. *Wear* **2004**, *257*, 509–522.
(35) Dai, H.; Rinzler, A. G.; Nikolaev, P.; Thess, A.; Colbert, D. T.; Smalley, R. E. *Chem. Phys. Lett.* **1996**, *260*, 471–475.
(36) Peigney, A.; Coquay, P.; Flahaut, E.; Vandenberghe, R. E.; De Grave, E.; Laurent, Ch. *J. Phys. Chem. B* **2001**, *105*, 9699–9710.
(37) de Resende, V. G.; De Grave, E.; Peigney, A.; Laurent, Ch. *J. Phys. Chem. C* **2008**, *112*, 5756–5761.
(38) Yoshihara, N.; Ago, H.; Masaharu, T. *J. Phys. Chem. C* **2007**, *111*, 11577–11582.
(39) Hata, K.; Futaba, D. N.; Mizuno, K.; Namai, T.; Yumura, M.; Iijima, S. *Science* **2004**, *306*, 1362–1364.
(40) Qiu, J. S.; Wang, Z. Y.; Zhao, Z. B.; Wang, T. H. *Fuel* **2007**, *86*, 282–286.